A&A 464, L21–L24 (2007)
DOI: 10.1051/0004-6361:20066963

Astronomy & Astrophysics

Letter to the Editor

Globular clusters and dwarf galaxies in Fornax

I. Kinematics in the cluster core from multi-object spectroscopy⋆,⋆⋆

G. Bergond[1,2,3], E. Athanassoula[4], S. Leon[5], C. Balkowski[2], V. Cayatte[6], L. Chemin[2], R. Guzmán[7], G. Meylan[8], and Ph. Prugniel[2,9]

[1] Instituto de Astrofísica de Andalucía, C/ Camino Bajo de Huétor 50, 18008 Granada, España
e-mail: gbergond@caha.es
[2] Observatoire de Paris, GEPI (CNRS UMR 8111 & Université Paris 7), 5 place Jules Janssen, 92195 Meudon, France
[3] Department of Physics and Astronomy, Michigan State University, East Lansing, MI 48824, USA
[4] Observatoire de Marseille, 2 place Le Verrier, 13248 Marseille Cedex 04, France
[5] Instituto de Radioastronomía Milimétrica (IRAM), Avda. Divina Pastora 7, local 20, 18012 Granada, España
[6] Observatoire de Paris, LUTH (CNRS UMR 8102 & Université Paris 7), 5 place Jules Janssen, 92195 Meudon, France
[7] Astronomy department, Univ. of Florida, 211 Bryant Space Science Center, PO Box 112055, Gainesville, FL 32611, USA
[8] École Polytechnique Fédérale de Lausanne (EPFL), Laboratoire d'Astrophysique, Observatoire, 1290 Sauverny, Suisse
[9] Centre de Recherches Astronomiques, Université Lyon 1, Observatoire de Lyon, 69561 Saint Genis Laval Cedex, France

Received 18 December 2006 / Accepted 11 January 2007

ABSTRACT

Aims. We acquired radial velocities of a significant number of globular clusters (GCs) on wide fields between galaxies in the nearby Fornax cluster of galaxies, in order to derive their velocity dispersion radial profile and to probe the dynamics of the cluster.
Methods. We used FLAMES on the VLT to obtain accurate velocities for 149 GCs, within a ≈500 × 150 kpc strip centered on NGC 1399, the Fornax central galaxy. These objects are at the very bright tail ($M_V \lesssim -9.5$) of the GC luminosity function, overlapping the so-called "ultra-compact dwarfs" magnitude range. Eight of the brightest FLAMES-confirmed members indeed show hints of resolution in the subarcsecond pre-imaging data we used for selecting the ∼500 targets for FLAMES spectroscopy.
Results. Ignoring the GCs around galaxies by applying $3d_{25}$ diameter masks, we find 61 GCs of $20.0 \leq V \leq 22.2$ lying in the intra-cluster (IC) medium. The velocity dispersion of the population of ICGCs is 200 km s^{-1} at ∼150 kpc from the central NGC 1399 and rises to nearly 400 km s^{-1} at 200 kpc, a value which compares with the velocity dispersion of the population of dwarf galaxies, thought to be infalling from the surroundings of the cluster.

Key words. galaxies: star clusters – galaxies: kinematics and dynamics – galaxies: elliptical and lenticular, cD – galaxies: dwarf – galaxies: individual: Fornax cluster

1. Introduction

Stars between galaxies in groups and in clusters have long been observed as a diffuse component – the intra-cluster (IC) light – originating from unresolved populations. A decade ago, the first Virgo IC objects were confirmed as planetary nebulae (PNe, Arnaboldi et al. 1996). Fornax, as the second nearest cluster of galaxies (20.1 Mpc, Dunn & Jerjen 2006), is the other ideal dense environment to search for different types of intracluster material.

Globular clusters (GCs) are among the best candidates for IC objects. Being compact stellar systems ($r_{\rm eff} \lesssim 5$ pc) of $-10 \lesssim M_V$, they can be detected by deep imaging as a swarm of point-like sources surrounding their host galaxies. Spectroscopic follow-up on 8–10 m telescopes makes them unique dynamical tracers in the outer halos of nearby galaxies, in particular early-types (e.g. Bergond et al. 2006).

West et al. (1995) (see also Muzzio 1987) argued that GC populations exist in the IC medium within groups and clusters of galaxies. In Fornax, the first ICGCs candidates were proposed by Bassino et al. (2003) in the surroundings of dwarfs, and were observed between giant galaxies by Bassino et al. (2006a). In Virgo, an ICGC population has been detected indirectly by wide-field imaging (Tamura et al. 2006) and four ICGCs have been partly resolved into stars in a recent HST/ACS observation (Williams et al. 2007). But, to date, no spectroscopically confirmed population of ICGCs has been found. Such objects would be "wandering" in the cluster potential well, probing it as a whole.

In this Letter, we present the results of a systematic search for ICGCs in the nearby Southern Fornax cluster, making use of wide-field images to select GC candidates and a medium resolution spectroscopic follow-up with FLAMES on the VLT.

2. The data and inferred GIRAFFE radial velocities

We give here only a very brief description of the observing runs, data reduction and analysis and will present more detailed information elsewhere. In a separate study

⋆ Based on observations collected at the ESO La Silla and Paranal observatories (programs 66.A–0345, 072.A–0389 and 074.A–0756).
⋆⋆ Tables 1–3 are only available in electronic form at http://www.aanda.org

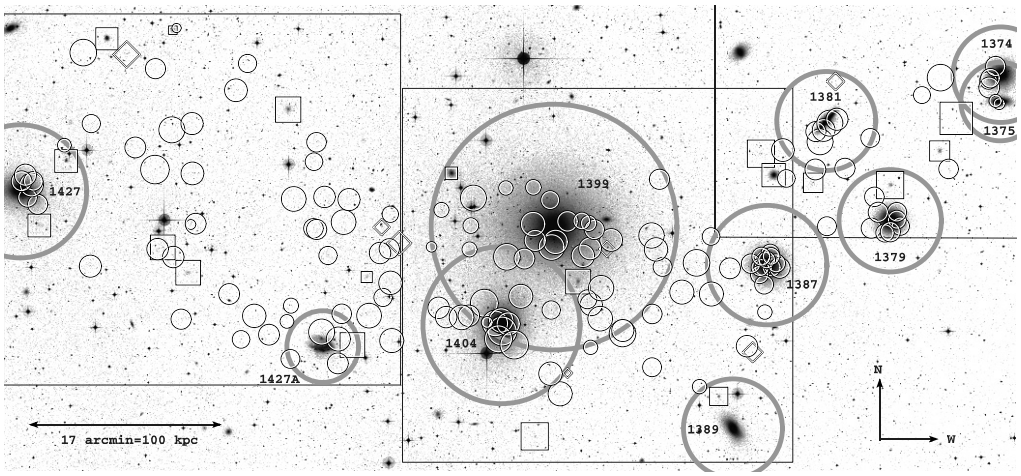

Fig. 1. DSS image of the 90′ × 40′ (∼530 × 230 kpc) central region of Fornax. The three WFI pre-imaging rectangular (sub-)fields are indicated. The large, bold grey circles around each NGC-labelled giant Fornax galaxy are the $3d_{25}$ diameter masks used to select ICGCs. Overlayed symbols are the FLAMES confirmed members: circles for the 149 (IC)GCs, squares for 19 Fornax dwarfs, and lozenges for 8 ultra-compact objects. Symbol size is proportional to the velocity, from 548 to 2373 km s^{-1}.

(Bergond et al., in preparation), we obtained deep, wide field images of a ∼0.°9^2 strip in Fornax, in $BV(R)I$, with the WFI mosaic camera at the La Silla ESO/MPG 2.2-m telescope. With its 34′ × 33′ field, WFI is particularly well-suited for selecting candidate (IC)GCs for spectroscopic follow-up studies. These are selected as point-like sources having $B - V$ and $V - I$ colours similar to Galactic GCs and $19.5 \leq V \leq 22.2$.

The spectroscopic follow-up was done using the GIRAFFE/MEDUSA mode of FLAMES, the multi-object fibre-fed spectrograph on the UT2 of the VLT. We allocated most of the 130 MEDUSA fibres which can be deployed in a 25′⌀ field to >100 of the WFI candidate GCs. Our magnitude selection criteria given above ensure that we get spectra of sufficient S/N in ∼4-h exposures with the LR4 grating. We completed the target list with slighlty resolved, $V \leq 20.5$ and $V - I < 1.5$ objects – candidate for ultra-compact dwarfs, see Sect. 4 – and with visually-selected dwarf galaxies, mostly dE,N. Five slightly overlapping FLAMES pointings, observed during two Paris Observatory GTO nights, cover a bended strip of ∼80′ × 25′ around NGC 1399 and include nine other giant Fornax galaxies (1′ ≃ 5.85 kpc at the adopted distance of 20.1 Mpc, Fig. 1).

A total of more than 500 WFI candidate GCs and dwarfs were followed-up. Data reduction of all spectra was performed with the IRAF HYDRA package, and radial velocities (v) computed by cross-correlation with the RV/`fxcor` task, using simultaneously obtained templates and 100 ÉLODIE library F5–K0 templates. Many Mg/Fe strong absorption lines fall in the ∼5000–5800 Å wavelength range of the LR4 grating used. According to the percentage of valid Gaussian fits to the cross-correlation function (CCF) peak, targets were allocated to three classes (A, B and C, similarly defined in Bergond et al. 2006) reflecting the quality of v estimates.

Class A objects represent very secure v estimates, where 98% or more of the ÉLODIE templates, as well as more than half of the simultaneous templates, agree within the velocity errors. Class B show 60%–97% ÉLODIE agreement but less than half of the simultaneous templates give consistent velocities. Class C have less than 60% agreeement between ÉLODIE templates; these possible members would require a definitive, independent confirmation (e.g. observations with other GIRAFFE gratings). These are mainly either metal-poor objects showing few lines in the LR4 grating range, or low signal ($S/N \lesssim 5$ per pixel) spectra from the faintest sources or from fibres located near the FLAMES field border where some vignetting and differential refraction induce flux lost. The astrometric accuracy of our input catalogue should not be at stake, as we obtained rms < 0.″2 w.r.t. the GSC2.1 and UCAC1 catalogues.

The typical error $\overline{\delta v}$ as estimated by `fxcor` is of the order of 10 km s^{-1}, and this is confirmed when comparing a dozen of objects in common between different FLAMES pointings. Velocities for the 15 GCs previously observed in other studies also fairly agree, FLAMES reducing the errors by a factor ∼2 to ∼10 w.r.t. the 9 GCs in common with Dirsch et al. (2004) and the 6 from Mieske et al. (2004a).

All Fornax members were selected in the velocity range $500 < v < 2500$ km s^{-1} (Drinkwater et al. 2001), giving a total of 149 (class A+B) GCs and 27 (all classes) dwarfs. In the finding chart (Fig. 1) and the kinematical analysis hereafter, we do not consider class C GCs (but keep class C dwarfs, due to small numbers). Our experience with various FLAMES datasets and CCF techniques makes us confident that all class A and almost all class B GCs and dwarfs are bona fide Fornax members. Moreover, excluding class B GCs in the following discussion does not change the main results. The coordinates and radial velocities of all detected members are given in Tables 1–3.

3. Intracluster globular cluster kinematics

We define as GCs the sources which are unresolved in the WFI study and whose velocities as found by FLAMES select them as Fornax members (Table 1). Note that only the bright tail of the GC populations ($M_V \lesssim -9.5$) can be observed by FLAMES because of the typical limiting magnitude $V \sim 22$. To our knowledge, 134 of these GCs were previously undetected, lying in particular at large distances from galaxies. Figure 1 nevertheless illustrates the clear concentration of GCs around the Fornax giant ellipticals. To select ICGCs, we mask out all GCs lying close to the ten giant galaxies in the FLAMES fields. We have taken the mask diameter to be $3d_{25}$, the latter obtained from HyperLEDA.

Using these criteria, we find that 61 GCs are part of the intracluster Fornax medium. The most striking examples are the GCs situated more than 200 kpc away – in projection – from NGC 1399; some of these "wanderer" GCs being located 100 kpc from any bright galaxy. Of course, by masking $1.5d_{25}$ around each of the galaxies we miss true ICGCs which are projected close to Fornax giants. The masked areas represent around a third of the total FLAMES coverage, so about 20 ICGCs should be occulted (considering they have an uniform spatial distribution). Compared to the 88 GCs we count within the $3d_{25}$

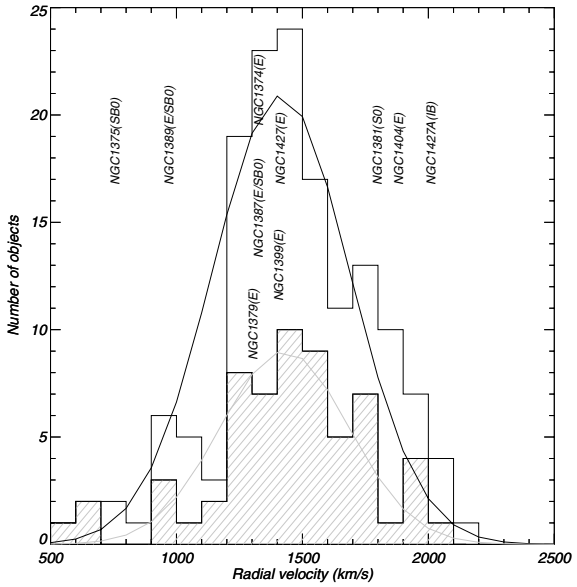

Fig. 2. Histograms of radial velocities for all 149 GCs in Fornax (solid line) and the subsample of 61 ICGCs (hatched area). Names of the main Fornax galaxies in our fields are located in abcissa at their systemic velocities, with the galaxy morphology following between parenthesis.

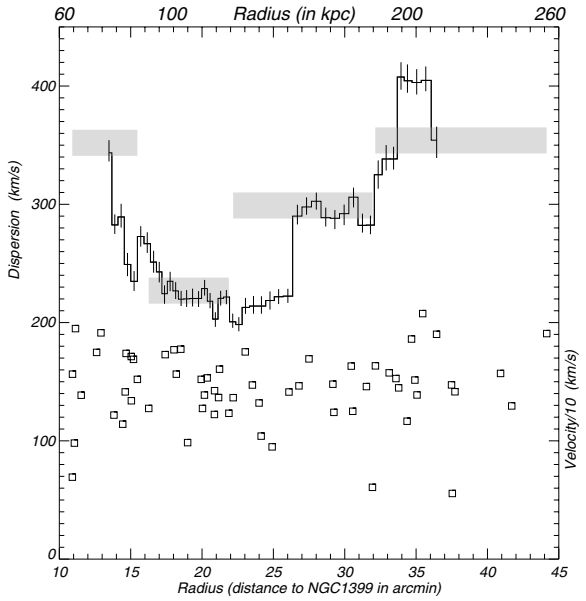

Fig. 3. Velocity dispersion σ_p radial profile for ICGCs in Fornax as a function of radius R (projected distance to NGC 1399), using a sliding window containing 20 ICGCs (black curve with error bars) as well as σ_p computed in 4 independent bins containing 15 ICGCs (16 for the outermost bin), shown in light grey; the height corresponds to the error on σ_p. The dip at ∼150 kpc might correspond to the transition from the baryonic mass profile of the central galaxy to its extended dark matter halo. Below the σ_p curve are shown the $v/10$ velocities of the 61 ICGCs.

of all ten galaxies, the masked area should therefore include around 23% contamination by projected ICGCs.

The histogram of the GC velocities (Fig. 2) shows that the velocity distribution of the ICGCs is more symmetric than that of the total GC population. The latter seems skewed by GCs with velocities around those of NGC 1404 and NGC 1427A, i.e. high w.r.t. that of the cluster. Fitting a Gaussian to each of the distributions, we find that the velocity peaks are similarly located at 1415 ± 7 (resp. 1429 ± 8) km s^{-1} for all (resp. IC) GCs, with a *FWHM* of 644 (resp. 602) km s^{-1}. The ICGC global projected velocity dispersion is $\overline{\sigma_p} = 312^{+8}_{-5}$ km s^{-1}.

Figure 3 shows the σ_p of ICGCs as a function of the projected distance to NGC 1399, R, as estimated within a sliding window including 20 GCs. This choice gives in each thus defined radial bin error bars ≲20 km s^{-1} (as estimated from bootstrap uncertainties). Overlayed (light grey bars) are the σ_p values computed in four independant radial bins of 15 GCs each (16 for the outermost one). Both estimates agree.

From 75 to 100 kpc a sharp decrease of $\sigma_p(R)$ is found, with a strong gradient of about −5 km s^{-1} kpc^{-1}. Between 100 and 150 kpc, $\sigma_p(R)$ remains rather constant around 200–220 km s^{-1}. On the contrary, after 150 kpc, σ_p is sharply increasing from a minimum of 200 km s^{-1}, to reach 400 km s^{-1} at R = 200 kpc, i.e. close to the cluster core (King) radius estimated in the visual Fornax Cluster Catalog (Ferguson 1989).

4. Ultra-compact objects and Fornax dwarf galaxies

In addition to unresolved GC candidates, we also targetted WFI slightly extended $V \leq 20.5$ sources, of $FWHM \leq 1''$ but SExtractor (Bertin & Arnouts 1996) stellarity index <0.3, candidates for the so-called "ultra-compact dwarfs" (UCDs, Phillipps et al. 2001; Drinkwater et al. 2003; Mieske et al. 2004a). Eight (five class A, see Table 2) of the 27 compact objects we observed have FLAMES velocities compatible with Fornax membership. Five of them were previously uncatalogued. These objects do appear resolved in our best (0.″7 seeing) I-band WFI images and correspond to subarcsec i.e. half-light radii <50 pc. It is worth mentioning that one of them would be located (at least) 200 kpc from the central NGC 1399; however this possible new UCD has not a well-determined velocity, as it lies on the limit between class B and class C objects, and needs further confirmation.

We also detect 19 (15 class A+B) "normal" dwarf galaxies in Fornax, mostly nucleated, 11 without previous velocity measurement (see Table 3). FLAMES Fornax dwarfs show a global velocity dispersion of 413 ± 9 km s^{-1}, in good agreement with the 429 ± 41 km s^{-1} value found by Drinkwater et al. (2001) for 55 dwarfs in the whole cluster.

5. Concluding remarks

The origin of ICGCs may be drawn from two main scenarios: (1) ICGCs are a primordial population, formed at high redshift at the very beginning of the Fornax cluster building-up, without being associated to any given galaxy; (2) ICGCs are GCs stripped from Fornax (possibly infalling dwarf) galaxies.

Using an average specific frequency (defined as the number of GCs per unit $M_V = -15$ of galaxy luminosity) of $S_N \sim 4$ for all giant galaxies in Fornax (Harris 1991), but excluding the central NGC 1399, we would expect to find roughly 500 GCs within $-11 < M_V < -10$. Within our spatial coverage, we should observe a maximum of about 30 such luminous GCs at radii larger than 50 kpc, assuming that stripped GCs follow the spatial distribution of galaxies. We count 20 such bright ICGCs beyond 50 kpc, which would imply a 66% stripping efficiency if it was the only process at play. This may be a lower estimate, considering the low S_N values found recently by Bassino et al. (2006b) for some early-types in our fields. Such a high stripping efficiency is unlikely and suggests that part of the ICGCs are a primordial intracluster population.

Nevertheless, stripping of GCs clearly appears ongoing in Fornax, as in the pass-by encounter of NGC 1399 and NGC 1404

(Bekki et al. 2003b). The high-velocity NGC 1427A (v = 2028 km s^{-1}) is also probably infalling towards the centre, considering its "blown-off" morphology. Georgiev et al. (2006) recently studied this LMC-like galaxy. Using their identification chart, four of their photometrically selected candidates are FLAMES-confirmed cluster members; in the same studied area, we find another they did not consider, being just brighter than their magnitude cut at $V = 21$. In such cases, an efficient stripping of GCs could naturally explain the high $S_N > 10$ of NGC 1399 (Hilker et al. 1999) (but see Dirsch et al. 2004; Forte et al. 2005), at the center of the potential well.

Our observations show that the inner ICGC population ($R <$ 150 kpc) has a velocity dispersion which decreases with radius, is likely relaxed and is still probably associated to the (outer) halo of NGC 1399. Beyond 150 kpc, a dynamically distinct, hotter population of GCs appears, with a velocity dispersion which increases with radius until, at around 200 kpc, it reaches the dispersion of Fornax dwarf galaxies, thus suggesting a link between them. Drinkwater et al. (2001) proposed an infall scenario to explain a higher velocity dispersion of 429 km s^{-1} for Fornax dwarfs on a much larger scale, compared to 308 km s^{-1} for giants members.

The most massive (IC)GCs might also be regarded as extremely compact dwarfs rather than stellar clusters; the nature of so compact stellar systems still being debated, UCDs may be considered as "transitional" objects. Indeed, Haşegan et al. (2005) called them DGTOs for Dwarf-Globular Transition Objects. UCDs were first discovered in Fornax (Hilker et al. 1999; Phillipps et al. 2001), but their existence is now confirmed in Virgo (Jones et al. 2006) and they are probably present in more distant clusters like Abell 1689 (Mieske et al. 2004b). It is not yet clear if UCDs are the remnant of dE(,N) tidally-truncated cores (Bekki et al. 2003a) or were formed by aggregation of star clusters (Fellhauer & Kroupa 2002). Another explanation could be that UCDs come simply from the direct evolution of very massive young clusters, as those formed in tidal tails of mergers (Kissler-Patig et al. 2006). UCDs may then be downscaled versions of the tidal dwarf galaxies found in the simulations of Bournaud & Duc (2006). Finally, Reverte et al. (2006) have recently discovered two ultra-compact H II, strong starburst regions in Hα images of two Abell clusters. Are they possible progenitors of UCDs?

Some authors tend to call "UCDs" all bright *unresolved* members in Fornax, so that they could rather be observing extremely bright but *genuine* GCs, like ω Cen in the Galaxy or Mayall II in M 31 (Meylan et al. 2001), which both exhibit some peculiarities but overall fit well within the GC locus in Kormendy's (1985) diagrams. Here, we have reserved a conservative definition of "ultra-compact" only for the sources resolved in our 0.″7 images. The definitive distinction between UCDs and GCs, if any, may only be done through high-resolution HST imaging and spectroscopy of all compact bright Fornax members, to estimate their central velocity dispersion and infer their mass-to-light ratios.

By means of wide-field VLT/FLAMES multi-object spectroscopy, we have confirmed 149 bright GCs and 27 (including 8 ultra-compact) dwarf galaxies as likely members of the Fornax cluster; 134 of those GCs were previously uncatalogued. The superb radial velocity accuracy (10 km s^{-1}, typically, up to $V \sim 22$ mag targets) and multiplexity-spatial coverage of FLAMES in its GIRAFFE/MEDUSA mode allows us to give quantitative results on the kinematics in the Fornax central E–W strip, up to 220 kpc i.e., one cluster core radius off the central NGC 1399. Considering in particular the 61 GCs lying beetwen the Fornax galaxies, we find that their velocity dispersion – after a decline from 350 to 200 km s^{-1} at what could be considered the vanishing NGC 1399 halo, around 150 kpc – next remarkably approaches 400 km s^{-1} at $R \sim R_c = 220$ kpc from it. This population of ICGCs could well not be relaxed yet.

It is tempting to compare the outermost ICGC dispersion to the value found for an infalling population of Fornax dwarf galaxies (Drinkwater et al. 2001). Other recent studies based on various techniques (distance determination via SBF, Dunn & Jerjen 2006; Scharf et al. 2005, X-ray gas properties) suggest that accretion/collapse is still ongoing in Fornax which thus appears to be a rather dynamically young, compact cluster. More FLAMES observations of globular clusters in the outskirts of Fornax, including towards the Fornax A (NGC 1316) subgroup, may definitely confirm this trend for such intergalactic globular clusters and provide new insights on the building-up of galaxy clusters.

Acknowledgements. We thank the referee, M. Drinkwater, for useful comments. We are indebted to Dominique Proust and Mathieu Puech for taking great care of the FLAMES observations during the two nights of GEPI/Observatoire de Paris guaranteed time used for this work. We acknowledge Francine Leeuwin for leading the imaging part of the project in its early beginnings. GB is supported at the IAA/CSIC by an I3P contract (I3P-PC2005-F) funded by the European Social Fund, with additional support by DGI grant AYA 2005-07516-C02-01 and the Junta de Andalucía. This work made use of the HyperLEDA database (`http://leda.univ-lyon1.fr`).

References

Arnaboldi, M., Freeman, K. C., Mendez, R. H., et al. 1996, ApJ, 472, 145
Bassino, L. P., Cellone, S. A., Forte, J. C., & Dirsch, B. 2003, A&A, 399, 489
Bassino, L. P., Faifer, F. R., Forte, J. C., et al. 2006a, A&A, 451, 789
Bassino, L. P., Richtler, T., & Dirsch, B. 2006b, MNRAS, 367, 156
Bekki, K., Couch, W. J., Drinkwater, M. J., & Shioya, Y. 2003a, MNRAS, 344, 399
Bekki, K., Forbes, D. A., Beasley, M. A., & Couch, W. J. 2003b, MNRAS, 344, 1334
Bergond, G., Zepf, S. E., Romanowsky, A. J., Sharples, R. M., & Rhode, K. L. 2006, A&A, 448, 155
Bertin, E., & Arnouts, S. 1996, A&AS, 117, 393
Bournaud, F., & Duc, P.-A. 2006, A&A, 456, 481
Dirsch, B., Richtler, T., Geisler, D., et al. 2004, AJ, 127, 2114
Drinkwater, M. J., Gregg, M. D., Hilker, M., et al. 2003, Nature, 423, 519
Drinkwater, M. J., Gregg, M. D., Holman, B. A., & Brown, M. J. I. 2001, MNRAS, 326, 1076
Dunn, L. P., & Jerjen, H. 2006, AJ, 132, 1384
Fellhauer, M., & Kroupa, P. 2002, MNRAS, 330, 642
Ferguson, H. C. 1989, AJ, 98, 367
Forte, J. C., Faifer, F., & Geisler, D. 2005, MNRAS, 357, 56
Georgiev, I. Y., Hilker, M., Puzia, T. H., et al. 2006, A&A, 452, 141
Haşegan, M., Jordán, A., Côté, P., et al. 2005, ApJ, 627, 203
Harris, W. E. 1991, ARA&A, 29, 543
Hilker, M., Infante, L., & Richtler, T. 1999, A&AS, 138, 55
Jones, J. B., Drinkwater, M. J., Jurek, R., et al. 2006, AJ, 131, 312
Kissler-Patig, M., Jordán, A., & Bastian, N. 2006, A&A, 448, 1031
Kormendy, J. 1985, ApJ, 295, 73
Meylan, G., Sarajedini, A., Jablonka, P., et al. 2001, AJ, 122, 830
Mieske, S., Hilker, M., & Infante, L. 2004a, A&A, 418, 445
Mieske, S., Infante, L., Benítez, N., et al. 2004b, AJ, 128, 1529
Muzzio, J. C. 1987, PASP, 99, 245
Phillipps, S., Drinkwater, M. J., Gregg, M. D., & Jones, J. B. 2001, ApJ, 560, 201
Reverte, D., Vílchez, J. M., Hernández-Fernández, J. D., & Iglesias-Páramo, J. 2006, ArXiv Astrophysics e-prints
Scharf, C. A., Zurek, D. R., & Bureau, M. 2005, ApJ, 633, 154
Tamura, N., Sharples, R. M., Arimoto, N., et al. 2006, MNRAS, 373, 601
West, M. J., Cote, P., Jones, C., Forman, W., & Marzke, R. O. 1995, ApJ, 453, L77
Williams, B. F., Ciardullo, R., Durrell, P. R., et al. 2007, ApJ, 654, 835

Online Material

Table 1. Fornax class A and B globular clusters confirmed by the FLAMES study, identified by their WFI source number with their J2000.0 coordinates, heliocentric radial velocity v and associated error δv as estimated by `fxcor`, as well as the resulting CCF fit $\mathcal{R}$ coefficient. The comments include a comparison with GCs observed in previous studies: Mieske et al. (2004a, prefix "fcos"), and Dirsch et al. (2004, prefix "dir"). Among the brightest objects, gc302.3, gc46.30, gc241.1, gc85.30 and gc271.5 show marginal signs of resolution, with *FWHM* about 10% larger than the seeing. Higher resolution data would be needed to classify them as likely new UCDs.

Id_{WFI}	α (J2000.0)	δ (J2000.0)	v (km s^{-1})	δv	$\mathcal{R}$	Class	Comments
gc302.3	03:37:43.560	−35:22:51.20	1419	11	6.8	A	
gc46.30	03:37:27.562	−35:30:12.54	1913	5	13.9	A	ICGC
gc241.1	03:39:17.672	−35:25:29.86	1027	8	10.9	A	fcos1-060 = 980 ± 45
gc76.40	03:36:57.252	−35:29:56.77	1246	7	16.7	A	
gc230.7	03:36:34.335	−35:19:32.58	1861	5	16.0	A	
gc85.30	03:37:45.066	−35:29:01.28	1657	9	7.6	A	
gc235.7	03:36:12.687	−35:19:11.57	1310	21	3.3	B	
gc41.40	03:36:51.638	−35:30:38.75	1468	17	4.9	A	
gc89.40	03:36:55.337	−35:29:37.71	1209	9	12.1	A	
gc271.5	03:37:05.708	−35:37:32.09	1520	7	8.6	A	ICGC
gc131.6	03:40:32.511	−35:36:23.04	1465	5	16.0	A	ICGC
gc199.6	03:40:22.907	−35:33:50.74	1040	5	12.5	A	ICGC
gc6.300	03:40:21.409	−35:24:27.64	1752	5	10.3	A	ICGC
gc129.2	03:41:29.535	−35:19:48.60	1473	6	10.6	A	ICGC
gc56.40	03:37:03.991	−35:30:16.48	1372	9	6.6	A	
gc323.6	03:35:21.541	−35:14:42.23	1464	5	14.8	A	
gc144.6	03:35:38.864	−35:21:53.40	1388	32	3.8	B	ICGC
gc35.30	03:37:42.235	−35:30:33.85	1319	9	7.1	A	fcos2-2094 = 1462 ± 121
gc44.40	03:37:00.037	−35:30:36.19	1268	13	7.4	A	
gc613.2	03:38:37.978	−35:23:32.57	1050	15	3.6	B	
gc317.2	03:38:11.700	−35:27:15.88	1434	8	6.6	A	fcos2-2127 = 1476 ± 201
gc381.6	03:37:46.708	−35:34:42.16	1386	13	4.2	B	ICGC; fcos2-086 = 1400 ± 50
gc248.7	03:36:32.793	−35:18:30.28	1611	6	11.6	A	
gc152.1	03:42:00.125	−35:19:32.49	947	15	3.2	B	
gc359.8	03:39:19.063	−35:34:06.66	1526	10	4.5	A	fcos1-2050 = 1635 ± 104
gc319.1	03:38:49.845	−35:23:35.56	972	16	4.3	A	dir76:63 = 933 ± 29, fcos1-064 = 900 ± 85
gc365.2	03:38:14.179	−35:26:43.35	1143	19	4.6	A	
gc324.8	03:39:06.040	−35:34:49.52	1540	10	4.4	A	
gc220.8	03:36:50.357	−35:20:16.82	1606	6	10.4	A	ICGC
gc69.20	03:41:05.011	−35:22:08.55	1634	8	7.5	A	ICGC
gc357.2	03:38:38.135	−35:26:46.39	1800	13	3.8	B	dir77:2 = 1815 ± 34
gc290.6	03:35:42.523	−35:13:51.71	1901	16	3.9	B	ICGC
gc396.2	03:38:17.075	−35:26:30.66	1235	12	6.0	A	dir82:57 = 1232 ± 22, fcos0-2089 = 1294 ± 95
gc69.70	03:36:01.104	−35:25:43.07	1389	8	11.0	A	
gc154.7	03:38:26.616	−35:41:42.96	1739	15	5.6	A	ICGC
gc216.7	03:38:30.776	−35:39:56.63	1676	9	5.1	A	
gc410.7	03:38:30.401	−35:34:20.49	1263	10	5.1	A	
gc70.50	03:40:02.811	−35:38:57.16	1467	5	13.2	A	
gc175.1	03:39:05.005	−35:26:53.47	1057	10	6.8	A	fcos0-2092 = 970 ± 205
gc346.6	03:35:21.028	−35:13:53.22	1374	6	15.6	A	
gc212.5	03:39:49.163	−35:34:46.17	1770	8	6.1	A	ICGC
gc272.7	03:36:27.090	−35:17:33.30	1573	10	8.0	A	
gc465.7	03:38:43.527	−35:33:07.70	1743	13	4.0	A	
gc269.8	03:38:53.244	−35:36:51.71	2000	13	4.7	A	
gc376.8	03:39:15.834	−35:34:55.97	1506	12	3.7	B	
gc155.4	03:37:21.301	−35:27:53.20	1218	12	5.8	A	ICGC
gc247.7	03:36:36.134	−35:18:38.60	1447	8	8.9	A	
gc445.7	03:38:09.204	−35:35:06.68	1773	22	4.0	B	
gc21.70	03:35:59.574	−35:26:56.58	1272	12	7.8	A	
gc260.7	03:36:30.136	−35:17:54.08	1879	7	10.3	A	
gc378.8	03:39:09.177	−35:34:57.94	1751	10	5.3	A	
gc555.2	03:38:30.730	−35:24:40.15	1323	24	4.2	A	dir77:40 = 1334 ± 13
gc362.5	03:36:58.015	−35:34:31.98	950	7	4.8	B	
gc398.5	03:37:21.128	−35:32:57.02	1713	11	5.5	A	ICGC
gc373.7	03:38:14.751	−35:33:24.32	1347	11	5.1	A	dir90:15 = 1298 ± 31
gc120.6	03:40:44.611	−35:36:46.74	1241	9	5.5	A	ICGC
gc156.2	03:38:13.538	−35:28:55.89	1606	14	4.8	A	
gc311.6	03:37:59.444	−35:36:09.18	1564	12	4.6	A	ICGC

Table 1. continued.

Id_{WFI}	α (J2000.0)	δ (J2000.0)	v (km s^{-1})	δv	$\mathcal{R}$	Class	Comments
gc61.10	03:38:49.499	−35:29:38.93	1949	12	3.6	B	
gc18.70	03:36:31.257	−35:26:58.22	1320	7	8.0	A	ICGC
gc107.4	03:36:55.732	−35:29:21.55	1260	6	12.1	A	
gc387.2	03:38:23.279	−35:26:32.72	1505	9	5.4	A	
gc428.7	03:41:20.356	−35:28:46.30	1514	6	10.3	A	ICGC
gc350.2	03:41:20.539	−35:12:53.66	1415	9	7.3	A	ICGC
gc388.5	03:36:58.337	−35:32:06.84	1314	10	6.2	A	
gc382.5	03:40:06.761	−35:29:27.32	1274	5	12.0	A	ICGC
gc153.8	03:36:48.830	−35:22:46.37	1223	7	9.7	A	ICGC
gc172.2	03:38:30.172	−35:28:47.81	1946	8	5.0	A	
gc115.3	03:38:04.436	−35:28:11.22	1624	15	5.7	A	dir91:109 = 1639 ± 19
gc133.3	03:37:47.017	−35:27:47.96	1835	20	4.2	B	
gc401.6	03:37:33.894	−35:32:46.91	1748	8	6.1	A	ICGC
gc159.5	03:40:02.534	−35:36:48.68	1741	6	11.3	A	
gc101.1	03:39:22.021	−35:28:44.79	693	7	4.3	B	ICGC
gc225.6	03:37:46.793	−35:39:23.54	1339	16	3.8	B	ICGC
gc280.1	03:39:03.854	−35:24:28.39	1880	16	3.6	B	
gc77.20	03:41:21.179	−35:21:46.23	2076	20	3.5	B	ICGC
gc236.6	03:40:49.601	−35:32:46.80	1479	5	13.0	A	ICGC
gc114.7	03:36:10.836	−35:24:22.46	1362	6	8.1	A	
gc152.5	03:39:39.420	−35:36:58.51	1729	7	8.4	A	ICGC
gc223.5	03:40:00.990	−35:34:35.59	1387	7	11.0	A	ICGC
gc12.70	03:36:12.131	−35:27:07.71	1419	6	8.9	A	
gc175.6	03:40:38.831	−35:34:43.12	1693	7	9.4	A	ICGC
gc300.6	03:37:59.568	−35:36:25.14	1949	9	4.8	B	ICGC
gc387.8	03:38:58.137	−35:35:24.77	785	9	6.2	A	
gc19.40	03:37:00.336	−35:31:13.97	1265	7	10.0	A	
gc289.7	03:38:46.424	−35:37:23.04	2052	10	5.6	A	
gc466.7	03:38:08.804	−35:32:25.53	1801	10	3.6	B	
gc91.20	03:38:41.920	−35:29:48.47	1484	9	3.8	B	
gc43.40	03:37:13.122	−35:30:41.35	1465	11	4.0	B	
gc221.2	03:38:37.212	−35:28:12.73	1578	15	5.5	A	
gc7.700	03:36:03.886	−35:27:26.42	1411	11	6.7	A	
gc280.7	03:38:13.399	−35:37:37.88	981	13	3.9	B	ICGC
gc414.7	03:38:59.310	−35:33:43.43	2016	15	3.7	B	dir84:11 = 2059 ± 28
gc102.2	03:38:16.653	−35:29:34.94	1669	9	4.6	B	dir89:74 = 1664 ± 28
gc71.60	03:40:23.320	−35:38:32.02	1301	8	8.8	A	
gc89.10	03:39:05.613	−35:28:59.31	1037	12	4.0	B	
gc212.2	03:38:28.441	−35:28:20.97	1804	19	3.9	B	
gc311.3	03:40:45.968	−35:14:51.64	1632	17	4.5	A	ICGC
gc177.6	03:37:26.253	−35:41:05.69	985	8	5.8	A	ICGC
gc90.40	03:36:59.578	−35:29:39.25	1304	7	7.6	A	
gc163.7	03:41:10.461	−35:34:57.47	1448	7	8.4	A	ICGC
gc417.5	03:39:39.759	−35:25:51.69	1141	15	4.5	A	ICGC
gc170.7	03:36:36.316	−35:21:58.68	1472	10	7.9	A	ICGC
gc395.7	03:41:03.826	−35:26:34.05	1459	8	6.3	A	ICGC
gc115.4	03:40:12.554	−35:21:11.72	1233	8	6.8	A	ICGC
gc2.100	03:42:11.924	−35:24:42.93	1413	9	5.5	A	
gc269.5	03:39:43.107	−35:33:10.41	1274	12	3.8	B	ICGC
gc4.700	03:36:06.204	−35:27:32.82	1252	9	4.8	A	
gc172.4	03:40:11.404	−35:19:29.25	1365	9	5.2	A	ICGC
gc345.7	03:38:13.066	−35:33:52.43	1566	10	3.4	B	dir90:9 = 1523 ± 29
gc70.70	03:36:09.122	−35:25:43.69	1403	8	5.9	B	
gc73.10	03:42:13.711	−35:22:41.10	1398	12	5.1	B	
gc302.6	03:35:50.492	−35:15:24.22	1166	6	8.0	A	ICGC
gc332.7	03:41:13.612	−35:29:28.90	1527	13	4.8	A	ICGC
gc30.60	03:35:21.876	−35:14:05.41	1249	16	4.4	B	
gc381.7	03:41:05.903	−35:26:38.00	607	9	6.2	A	ICGC
gc172.2	03:41:13.713	−35:18:17.44	1861	9	3.9	B	ICGC
gc317.5	03:39:39.846	−35:31:53.61	1689	11	7.3	A	ICGC
gc201.1	03:41:48.413	−35:17:40.25	1295	10	6.7	A	ICGC
gc304.8	03:41:49.465	−35:30:12.68	1570	12	3.1	B	ICGC
gc32.10	03:42:16.258	−35:24:06.13	1399	12	5.6	A	
gc13.40	03:40:08.114	−35:24:18.05	1532	8	8.6	A	ICGC
gc173.7	03:36:23.575	−35:21:52.32	1413	10	6.0	A	ICGC
gc459.5	03:40:12.978	−35:27:03.48	1366	9	7.2	A	ICGC
gc57.40	03:36:53.187	−35:30:14.43	1342	16	6.9	A	

Table 1. continued.

Id_{WFI}	α (J2000.0)	δ (J2000.0)	v (km s^{-1})	δv	$\mathcal{R}$	Class	Comments
gc85.10	03:42:17.040	−35:22:08.41	1578	11	7.0	A	
gc164.6	03:40:24.712	−35:35:13.69	949	10	5.6	A	ICGC
gc173.5	03:40:09.731	−35:36:11.17	1898	9	5.2	A	
gc39.70	03:36:01.107	−35:26:22.28	1324	19	5.9	A	Asymetric CCF
gc516.5	03:39:40.293	−35:28:53.71	1414	14	4.1	B	ICGC
gc6.400	03:39:57.562	−35:24:33.00	1564	9	4.9	A	ICGC
gc67.10	03:42:14.505	−35:23:00.09	1708	12	3.9	B	
gc325.6	03:35:18.844	−35:12:51.13	1429	13	4.5	A	
gc391.5	03:39:44.276	−35:29:15.90	1520	10	6.8	A	ICGC
gc441.5	03:39:59.951	−35:26:31.57	1775	9	4.5	A	ICGC
gc388.2	03:41:11.311	−35:09:20.21	555	12	4.0	B	ICGC (fcc160 GC?)
gc398.3	03:40:40.878	−35:12:30.49	1250	11	3.4	B	ICGC
gc74.10	03:42:18.711	−35:22:40.23	1468	13	4.7	A	
gc375.1	03:41:51.519	−35:11:24.91	1907	27	2.9	B	ICGC
gc467.5	03:40:11.597	−35:27:09.52	1424	9	6.0	A	ICGC
gc187.2	03:41:05.002	−35:17:45.30	1575	12	4.1	B	ICGC
gc1387se	03:36:58.701	−35:30:36.21	1273	7	17.9	A	
gc1387sw	03:36:55.132	−35:30:35.93	1340	10	11.5	A	
gc1404e	03:38:54.587	−35:35:30.18	1911	44	4.7	A	
gc1404n	03:38:52.046	−35:35:14.81	1816	16	9.1	A	
gc1404s	03:38:51.609	−35:36:10.49	2174	16	4.3	B	
gc1404w	03:38:49.016	−35:35:33.05	1730	36	3.4	B	
gc1375s	03:35:17.214	−35:16:07.65	785	12	8.5	A	Broad CCF
gc1375e	03:35:18.768	−35:15:53.06	852	6	14.5	A	

Table 2. Fornax class A and B ultra-compact objects confirmed by the FLAMES study, identified by their WFI source number with their J2000.0 coordinates, heliocentric radial velocity v and associated error δv as estimated by `fxcor`, as well as the resulting CCF fit $\mathcal{R}$ coefficient. The comments include a comparison with objects observed in previous studies: Phillipps et al. (2001, prefix "2dF"); Mieske et al. (2004a, prefix "fcos"); Dirsch et al. (2004, prefix "dir").

Id_{WFI}	α (J2000.0)	δ (J2000.0)	v (km s^{-1})	δv	$\mathcal{R}$	Class	Comments
ucdB	03:39:35.920	−35:28:24.59	1878	5	15.8	A	fcos1-2083 = 1848 ± 85, 2dF = 1920 ± 40
uc218.7	03:38:23.416	−35:39:53.32	757	21	3.8	B	
uc257.5	03:37:03.233	−35:38:04.37	1551	5	18.6	A	fcos2-2031 = 1571 ± 75, 2dF = 1491 ± 39
uc329.7	03:36:27.711	−35:14:13.91	1386	4	29.6	A	
uc411.2	03:41:32.855	−35:11:37.30	2076	11	3.3	B	
uc464.5	03:39:43.521	−35:26:59.25	1274	7	9.3	A	
uc82.40	03:36:58.524	−35:29:45.37	1379	19	5.2	B	In NGC 1387?
ucdA	03:38:06.298	−35:28:58.49	1234	5	17.3	A	fcos2.2111 = 1280 ± 58, dir91:93 = 1247 ± 16, dir90:86 = 1218 ± 9

Table 3. Fornax FLAMES dwarves (all classes). Names are from Ferguson (1989) or "newdw" for the newly detected dwarves, with the J2000.0 centre coordinates, heliocentric radial velocity v and associated error δv as estimated by `fxcor`, as well as the resulting CCF fit $\mathcal{R}$ coefficient. The comments include a comparison with velocities available in the literature, when available.

Name	α (J2000.0)	δ (J2000.0)	v (km s^{-1})	δv	$\mathcal{R}$	Class	Comments
fcc208	03:38:18.791	−35:31:50.69	1756	9	5.8	A	1720 ± 50
fcc194	03:37:17.933	−35:41:57.30	1295	15	4.3	A	1237 ± 84
newdw1	03:41:18.114	−35:28:37.46	1750	15	4.0	B	Previously uncatalogued
fcc259	03:41:07.230	−35:30:52.10	1770	17	3.5	B	1st velocity determination
fcc227	03:39:50.085	−35:31:22.27	700	50	2.5	C	1st velocity determination, very uncertain
fcc241	03:40:23.535	−35:16:35.86	1824	7	10.2	A	2045 ± 107
fcc1554	03:41:59.442	−35:20:56.18	1612	4	21.8	A	1642 ± 52
newdw2	03:39:56.441	−35:37:20.83	1770	14	4.0	C	Previously uncatalogued
fcc266	03:41:41.327	−35:10:13.26	1555	3	30.3	A	1551 ± 39
fcc160	03:41:12.880	−35:09:31.48	548	8	7.9	A	1493 ± 59
fcc272	03:42:11.300	−35:26:35.00	1608	15	4.5	B	1st velocity determination
fcc160	03:36:04.050	−35:23:20.00	1955	8	7.1	A	1st velocity determination
fcc171	03:36:37.270	−35:23:09.25	1395	5	12.0	A	1st velocity determination
newdw3	03:36:59.800	−35:20:36.00	1964	30	3.6	B	Previously uncatalogued
newdw4	03:35:35.670	−35:17:26.50	2373	14	3.7	C	Previously uncatalogued
fcc182	03:36:54.303	−35:22:28.78	1693	3	43.4	A	1669 ± 11
fcc156	03:35:42.750	−35:20:18.80	1405	22	2.8	C	1st velocity determination
fcc215	03:38:37.655	−35:45:27.39	1964	20	3.7	B	1st velocity determination
fcc222	03:39:13.319	−35:22:16.74	800	5	12.8	A	792 ± 26